Beacons of Life from Exoplanets Around G and K Stars

Vladimir S. Airapetian[1], Charles H. Jackman[1], Martin Mlynczcak[2], William Danchi[1], Linda Hunt[3]
[1]NASA/GSFC, [2]NASA/LARC, [3]SSAI

Abstract

The current explosion in detection and characterization of thousands of extrasolar planets with the *Kepler* mission, the *HST,* and large ground-based telescopes opens a new era in searching for Earth analogs suitable for sustaining life. Recent studies show that the frequency of occurrence of small terrestrial type planets around G, K, and M dwarfs is over 10% [1]. As more Earth-sized exoplanets are detected in the near future, we will soon have an opportunity to identify habitable worlds. How should we search for biological signatures of life (or biosignatures) in habitable planets with our current capabilities? In order to find signatures of life on terrestrial type planets we need to identify and detect chemical compounds in their atmospheres that are associated with life forms. The detection of the proposed bio-signatures including O_2, O_3, H_2O, CH_4 requires weeks of integration time with largest space telescopes, and thus are currently very challenging for current instruments. Here we propose to use a powerful broad-band emission of nitric oxide (NO) molecule at 5.3 μm, hydroxyl (OH) at 1.6 and 2 μm and molecular oxygen (O_2) at 1.27 μm as signatures of nitrogen, oxygen, ozone and water rich atmospheres of terrestrial type exoplanets around young active G and K stars. These signals open a unique opportunity to perform direct imaging observations of Earth-sized exoplanets with high signal-to-noise and low spectral resolution with JWST-type mid-IR mission to detect fundamental prerequisites for life we term “beacons of life”.

1. Introduction.

The current methodologies for detecting observable signatures of life on terrestrial-type planets are based on chemical compounds in their atmospheres that are out of chemical equilibrium from the chemical processes modified by life [2,3]. Signatures of life as we know it (or biosignatuires) can be identified with remote-sensing detection of the most common molecules in the Earth's troposphere, including molecular oxygen (O_2), ozone (O_3), water vapor (H_2O), nitrous oxide (N_2O), and methane (CH_4), surface reflectance signatures or polarized scattering in exoplanetary atmospheres [4-6]. The presence of molecular oxygen, a strong marker of the presence of oxygen producing forms of life, together with methane, the marker of biological decay, and other molecules would suggest that the atmosphere is in chemical disequilibrium driven by biological activity [3, 5]. However, direct detection of molecular oxygen in the atmospheric band (around 760 nm), methane and other species through transmission spectroscopy during planetary transits requires many days of observations with extremely large ground-based and future space telescopes. Moreover, depending on the height of the atmosphere the abundance of some biomarkers including O_2 could be driven either by biological activity or abiotic processes via solar X-ray and extreme UV (*XUV*) fluxes and precipitating particles due to dissociation of carbon dioxide, water vapor or in the upper atmosphere of an exoplanet and can create false positive biosignatures [7-9].

Here, we propose to use non-thermal emission from broad molecular bands in the near- and mid-infrared (mid-IR) referred to as "beacons of life" from nitric oxide, hydroxyl and molecular oxygen as the strongest signals that may be observable from the habitable worlds.

2. Beacons of Life from Earth.

Life as we know it requires a nitrogen-rich atmosphere with the presence of oxygen produced by life-associated processes. Nitrogen is the most abundant molecule in the Earth's atmosphere. Its high abundance was critical for the initiation of life on Earth, because fixation of nitrogen is required to create linkages of long chained molecules including proteins and base pairs of RNA and DNA [10,11]. The three molecules NO, N_2O and HCN are necessary in intermediate chemical steps to create RNA. The molecule N_2O is a very potent greenhouse gas that has a potential to resolve the Faint Young Sun (FYS) paradox to warm the young Earth. Also, it is crucial for the production of abundant hydrogen cyanide, HCN, in the lower atmosphere, a precursor for prebiotic chemistry and life [11,12]. Byproducts of molecular nitrogen, molecular oxygen and water vapor formed due to interaction of solar photolyzing radiation can be found in the form of nitric oxide, NO, and hydroxyl, OH. Nitric oxide is efficiently produced in the thermosphere as a result of photo-dissociations (*X-ray* and *EUV*) and collisional dissociations (via precipitating electrons) of these major species through (see ***R1-R**** in the Supplemental Material).

Observations made over the last 15 years with the Sounding of the Atmosphere using Broadband Emission Radiometry (SABER) instrument aboard NASA's TIMED (Thermosphere Ionosphere Mesosphere Energetics Dynamics) satellite have revealed that Earth's thermosphere is a source of time-varying emission flux of NO at 5.3-μm, OH at 1.6 and 2 μm and O_2 ($^1\Delta$) at 1.27 μm. NO emits at 5.3-μm band via a large number of vibration-rotation transitions excited by inelastic collisions with atomic and molecular oxygen [13,14] and exothermic reactions. The emitting power of NO is strongly correlated with the solar activity cycle traced by the solar radio flux at

10.7 cm, the indicator of solar activity as well as the indices that trace the strength of Coronal Mass Ejection (CME) induced geomagnetic storms. The total power emitted by thermospheric nitric oxide at 5.3 μm and carbon dioxide at 15 μm can reach ~ 2 TW during the peak strong storms, one that occurred on Oct 28-31, 2003. This is a factor of 20-30 greater than the power emitted in those bands during the quiet Sun at solar minimum [14]. The Michelson Interferometer for Passive Atmospheric Sounding (MIPAS) observations reveal an increase of NO abundance by a factor of 10 at height range 6-68 km during large Oct-Nov 2003 geomagnetic storm [15]. Thus, the radiative power increase during geomagnetic storms is attributed to the enhancement of production of NO molecules and increased kinetic temperature. No infrared cooling plays the role of an efficient thermostat by cooling the thermosphere in response to the radiative and non-radiative heating associated with space weather events [16,17]. NO radiative cooling becomes sharply enhanced (more than a factor of 10) enhanced due to the increased energy input into the ionosphere-thermosphere (IT) system of polar cap regions during geomagnetic storms. The non-radiative heating is introduced by resistive dissipation of ionospheric currents (Joule heating, JH) in response to the perturbation of the global magnetosphere caused by CME events, ion-neutral collisions and particle precipitation in the polar regions of the planet. If most of the energy entering the I-T system is radiated away in the form of NO and CO_2 emission, then we can expect that its power should increase proportionally with the input energy flux. The *XUV* flare emission at wavelengths between 1-70 Å is another crucial source of production of low-latitude thermospheric NO driven by photoelectrons formed via photoionization of atmospheric species [18].

The time variations of the NO emission power at 5.3 μm derived from the long-term series of observations were parametrically fit with F10.7 flux, the measure of the solar XUV

flux, and Ap index, the measure of the geomagnetic activity. The young magnetically active solar-like stars of K and G spectral types generate the XUV flux in the transition region and coronal layers driven by magnetic heating processes, which is by a factor of 10 - 20 greater than that of the current Sun [19]. As a result, the planetary thermosphere responds back with the enhanced radiative cooling in the form of NO at 5.3 μm, CO_2 at 15 μm and conductive cooling. Thus, the total power of NO at 5.3 μm emitted by an exoplanet with the Earth's mass, atmospheric pressure and chemical composition (Earth twin) around an active star is expected to be on the order of ~10^{20} erg/s or a factor of 3 larger than the largest single value observd from Earth.

The emission in OH bands (1.6 & 2 μm) observed by SABER has the total power of ~ 0.2 TW, which is weakly dependent on the solar cycle (see *Figure 1*). Figure 2 presents the flux evolution of O_2 ($^1\Delta$) emission flux at 1.27 μm during 2004 to 2008, which shows variations of emission power between zero (at night, increasing substantially in daytime due to O_3 photolysis via UV solar radiation) to 230 TW.

3. Beacons of Life from Exoplanets Around Active Stars.

What NO and OH radiative fluxes are expected from Earth twins around active G and K stars? Depending on their age and spectral class, XUV fluxes from active stars resembling our Sun at 0.7 Gyr at the inner edge of the climatological habitable zones may vary from 1 to 10-20 times of the current Sun. To investigate the atmospheric chemistry changes owing to CME driven solar energetic particles (SEPs), we computed a grid of 5 atmospheric chemistry models of an Earth twin to numerically study the chemical evolution of nitrogen oxides, NO_x (N (^{4}S), N

(^{2}D), NO, NO_2, NO_3), HO_x (H, OH and HO_2) constituents and ozone in response to various fluxes of energetic protons during SEPs in its upper stratosphere. For this purpose, we used our two-dimensional photochemical transport Goddard Space Flight Center (*GSFC*) atmospheric model that calculates the constituents in the upper stratosphere (35 km) extending to the upper mesosphere (95 km) [20, 21] (see Supplemental Material). The solar particle fluxes were used to compute ion pair production profiles using the methodology proposed by [21, 22]. Our study includes the base model (base Model A, no SEP and the current XEUV flux, F_0), Model B (no SEP and XUV flux at $10F_0$), Model C (July 2000 SEP event and XUV flux at $10F_0$), Model D (10 x July 2000 SEP event and XUV flux at $10F_0$), Model E (20 x July 2000 SEP event and XUV flux at $10F_0$). We used the maximum daily average particle input for the SEP event, which occurred on July 15, 2000, that was associated with the fast (1800 km/s) halo CME and the Bastille Day X5.7 solar flare [23].

Our simulations suggest that at the height range between 0 to 95 km, the enhanced XUV flux from the Sun is not efficient in fixating molecular nitrogen, and thus only modest changes in NO mixing ratio are observed. Model B (no SEP and the active Sun at $10F_0$) shows NO values of typically 1 ppbv at 80-90 km (the left panel of Figure 3), which are similar to those computed for base Model A. The steady state energy flux in the form of energetic protons from 1-300 MeV with the energy spectrum and intensity characteristic for July 2000 SEP event (Model C, see also Supplemental Materials) produces the mixing ratio of NO that is enhanced by a factor of 200 (or 200 ppbv at the reference height of 85 km) in the polar cap regions (the middle panel of Figure 3) with respect to the quiet conditions described by Model B. Model D suggests that NO net production increases approximately linearly in response to the enhancement of the intensity of the proton flux by a factor of 10 with respect to Model C, and reaches 2 ppmv (the right panel of

Figure 3). These fluxes are consistent with the results of 1D atmospheric models applied for SEP driven atmospheric chemistry of exoplanets around M dwarfs [24]. Model E results show that this trend continues as we increase the proton flux by another factor of 2. Thus, we conclude that the net production of NO is scaled approximately linearly with the incident proton flux. This could be understood, because 70 to 80 % of the energy of incoming protons goes into creation of ionization pair production. Neutral and ion chemistry resulting from the ion pair production (that forms secondary electrons and ions) creates about 1.25 N and about 2 HO_x constituents and the proton impact of N atom production is divided between the ground state N(^{4} S) (45 % or 0.55 per ion pair) and excited state N(^{2}D) (55 % or 0.7 per ion pair) nitrogen atoms [25].

The increase of NO mixing ratio by 2 to 3 orders of magnitude is driven by the corresponding flux of precipitating protons produced by CME initiated shocks and associated secondary electrons. Each SEP associated CME event exerts a dynamic pressure on the planetary magnetosphere, which perturbs the geomagnetic field and induces geomagnetic currents in the polar regions. The resistive dissipation of these currents heats the ionosphere. The height integrated Joule heating (JH) rate introduced by such currents varies from a few mW/m^2 (for a regular CME event with the energy of 10^{31} ergs) to up to 1 W/m^2 for a super Carrington event with the energy of 2 x 10^{33} ergs [27,28]. The JH rate increased by 3 orders of magnitude should be balanced by the radiative and conductive cooling rates. The radiative cooling rates are mostly controlled by the enhanced emission from NO molecules due to enhanced production of NO due to SEP mediated dissociation. The generation of large amounts of NO has been shown in Earth's atmosphere to lead to "overcooling" events [29]. That is, so much NO is generated that the resultant infrared cooling leaves the atmosphere colder than it was before the geomagnetic event. NO emission at 5.3 μm is driven by collisional impact with atomic oxygen, and therefore, is

dependent on thermospheric abundance of O. Figure 1 (see Supplemental material) hows efficient production of atomic oxygen due to XUV flare emission from an active star (Model B) by a factor of 10^4. This is consistent with destruction of ozone by 90% in the polar regions of the planet due to photolysis and collisional dissociation as well as NO and

The O2 signal is proportional to J [O_3], where J is the ozone photolysis rate, [O_3] is the abundance of O_3. The ozone abundance also depends on more O_2 photolysis, it is inversely dependent on temperature, and also on the H, NO, NO_2, and other chemical abundances. Our Models C and D show that ozone is destroyed efficiently (up to 90%, see Figure 3 of Supplemental Material) both due to ozone photolysis and collisional dissociation with energetic particles, which increases production of O respectively.

The NO radiative cooling is temperature dependent (~ exp(2700/T)) and the rapid cooling cuts off the infrared emission – this is a manifestation of the "thermostat" effect discussed above. More detailed modeling of the response of Earth-like planets is required to understand whether NO emission would be prolonged after storms or rather would be short-lived due to overcooling.

The same linear scaling is observed for the increase of steady state resultant mixing ratios of production of HO_x (H, OH and HO_2) due to dissociation of water vapor via the incoming flux of SEP protons. Figure 4 shows the 2D maps of the OH mixing ratios for the models B, C and D (as in Figure 3). One can see that the mixing ratio for Model C increases to 100 ppbv at the reference height. As discussed in [26], most of produced OH represent vibrationally excited hydroxyl molecule, and thus expected radiative power at 1.6 μm and 2.0 μm should increase accordingly by the same factor if a sufficient amount of ozone is available to promote its production.

We point out that understanding the response of planetary upper atmosphere to strong CMEs is still a frontier of research even for the Earth. The current Decadal Survey [http://nap.edu/13060] for Solar and Space Physics identifies this topic as a Key Science Goal for Earth's thermosphere and ionosphere.

Such an increase implies the total NO emitting flux at 5.3 μm from the planet around an active K to G star (Models C and D) with an N-O_2 rich atmosphere is expected to be ~ 10^{20} -10^{22} erg/s. This is consistent with the estimate of the NO power at 5.3 μm during higher stellar activity expected from younger G and K type stars obtained from the linear scaling between X-ray flux (0.1-0.8 nm) GOES measurements with F10.7 flux obtained in [14] extended to F10.7 = 2000. The emission power from OH bands – 2 x 10^{18} – 10^{20} ergs/s and O_2 at 1.27 μm at least at the level of 2 x 10^{21} ergs/s.

For a planetary system located at 10 pc away from Earth, this implies the total flux at Earth integrated over the NO band with the band-width of ~ 5600 Å at 10^{-20} – 10^{-18} ergs/cm^2/s, the OH bands with the bandwidth of ~ 2000 Å at 2 x 10^{-22} – 10^{-20} erg/cm^2/s and O_2 band over the spectral width of 431 Å at ~ 2 x 10^{-19} ergs/cm^2/s. This suggests that lower spectral resolution $\lambda/\Delta\lambda$ =10 - 40 would be required to detect emission from these bands. The low spectral resolution ($\lambda/\Delta\lambda$ ~20) observations at the signal-to-noise of 10 will require only 1.5 hours of exposure time with a JWST/MIRI-type spectrograph at ~ 5 μm. Thus, if future space telescopes have apertures larger than JWST by a factor of 2, the exposure time could be reduced by a factor of 4 and the planets with the 10 times lower NO flux can be detected in just 4 hours. Because the emission flux from NO, OH and O_2 ($^1\Delta$) bands are dependent on stellar activity levels driven by geomagnetic storms & XUV flux, it is expected to vary on a time scale of storms, or ~ 2-3 days. This time should be shorter than the expected exposure time. The estimated number of prime Earth twin targets

around GK stars in the neighborhood of 10 pc for the detection of the beacons of life is at least ~ 20 planets [30, 31].

Although the raw signal itself from NO is observable as noted above, however, its size is small compared to the thermal emission from the exoplanet, $\sim 10^2$ larger, and much smaller than the emission from the host star, which can be $\sim 10^6$ greater for a star similar to the Sun. Thus, a possible observational strategy available in the near term, using JWST, would be to perform eclipse spectroscopy, where thermal emission from the exoplanet is observed, on a somewhat larger exoplanet, such as a super-Earth or mini-Neptune, around a smaller star like a late M dwarf. In this case, the signal is of the order of $10^{-2} - 10^{-3}$, and the spectral feature is of the order of $10^{-3} - 10^{-4}$ [32, 33], allowing a detection with a modest number of eclipses. Potential targets could be found by TESS and then observed with JWST. Ideally the host star would be known to be active, and, if possible, observed close in time by optical or UV observatories to correlate the eclipse observations with recent activity. The proposed "beacons of life" can be observed using direct imaging techniques in the mid IR bands via recently proposed "Exo-Life Beacon Space Telescope", an extended version of *FKSI* space interferometer [34,35].

Figures.

Figure 1. *Total emission power (in units of 0.1 TW): upper panel: OH (9→7 + 8→6) at 2 μm; lower panel: OH(5→3 + 4→2) power at 1.6 μm*

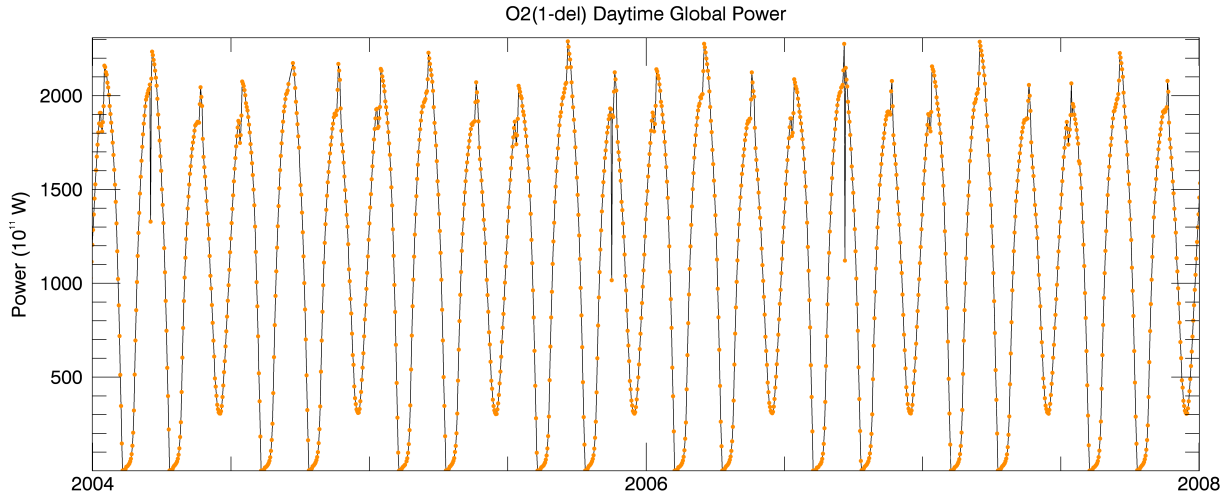

Figure 2. *The daily averages of the total emitting power (in units of 0.1 TW) by the Earth as a dot from $O_2(^1\Delta)$ at 1.27 μm*

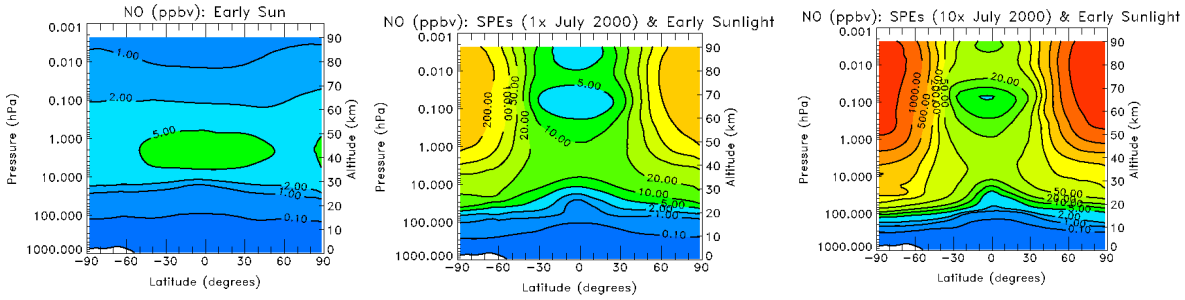

Figure 3. *2D map of steady state NO mixing ratio (in ppbv): Model B (left panel), Model C (middle panel) and Model D (right panel); Contour level: 0.1,1,2,5,10,20,50,100, 200,500, 1000, & 2000 ppbv*

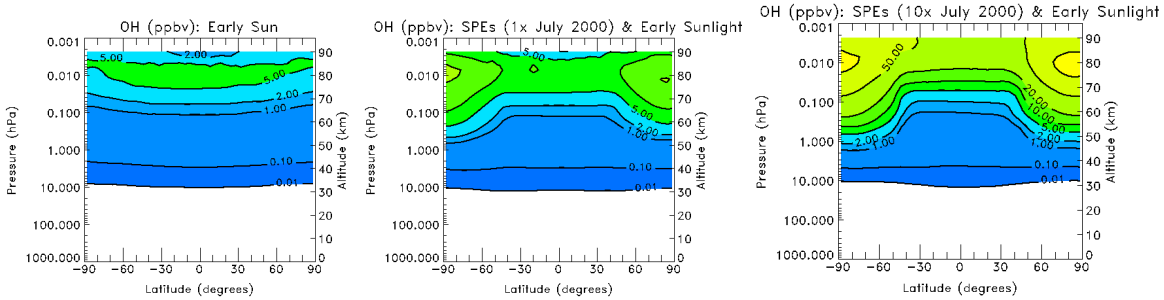

Figure 4. *2D map of steady state OH mixing ratio (in ppbv): Model B (left panel), Model C (middle panel) and Model D (right panel); Contour level: 0.1,1,2,5,10,20,50,100 ppbv*

References

1. Mullally, F., Coughlin, J. L., Thompson, S. E., et al. 2015, ApJS, 217, 31
2. Seagar, S. *Science*, 340, 577 (2013)
3. Lovelock, J. E. Proc. R. Soc. Lond. B, 189, 167 (1975)
4. Kaltenegger, L., Traub, W. A., Jucks, K. W. *ApJ*, 658, 598 (2007)
5. Seager, S., Bains, W., Petkowski, J. J.. Astrobiology, 16, 465 (2016)
6. Berdyugina, S. V. JQSRT, accepted (2016)
7. Seagar, S. *PNAS*, 111, 12635 (2014)
8. Arnold, L. et al. A&A, 564, A58 (2014)
9. Schwieterman, E. W., Meadows, V. S., Domagal-Goldman, S. D., Deming, D., Arney, G. N., Luger, R., Harman, C. E., Misra, A., Barnes, R. *ApJ Let*, 819, L13 (2014)
10. Cockell, S. *Phil. Trans. Roy. Soc.* 372, 20130082 (2014)
11. Benner, S. A., Kim, H J., Carrigan, M. A. Acc. Chem. Res. 45(12), 2025 (2012).
12. Airapetian, V., Glocer, A., Gronoff, G., E. Hébrard, E., Danchi, W. *Nature Geoscience*, DOI:10.1038/NGEO2719 (2016)
13. Mlynczak, M. G., Hunt, L. A., Thomas M., B. and 13 coauthors *JGR*, 115, Issue A3, CiteID A03309 (2010)
14. Mlynczak, M. G., Hunt, L. A., Marshall, B. T., Russell, J. M., Mertens, C. J., Thompson, R. E., Gordley, L. L. *GeoRL*, 42, Issue 10, 3677 (2015)
15. Lopez-Puertas, M., Funke, B., Bil-Lopez and 6 co-authors, *JGR*, 110, A09S43 (2005)
16. Verkhoglyadova, O. P., Tsurutani, B. T., Mannucci, A. J., Mlynczak, M. G., Hunt, L. A., Paxton, L. J., Komjathy, A. *JGR*, 121, 8900 (2016)
17. Knipp, D. J., Pette, D. V., Kilcommons, L. M., Isaacs, T. L., Cruz, A. A., Mlynczak, Hunt, L. A., Lin, C. Y. Space Weather, 15, doi:10.1002/2016SW001567 (2016)

18. Rodgers, E. M., Bailey, S. M., Warren, H. P., Woods, T. N., Eparvier, F. G. Adv. Space Res., 45, 28 (2010)

19. Güdel, M. & Nazé, Y. *A&A Rv*, 17, 309 (2009)

20. Jackman , C. H., Douglass, A. R., Rood, R. B., McPeters, R. D., Meade, P. E. JGR, 95, 7417 (1990)

21. Fleming, E. L., Jackman, C. H., Stolarski, R. S., Douglass, A. R. Atm. Chem. Phys., 11, 8515 (2011)

22. Vitt, F. M., Armstrong, T. P., Cravens, T. E., Dreschhoff, A. M., Jackman, C. H., Laird, C. M. *JASTP*, 62, Issue 8, 653 (2000)

23. Andrews, M. D. *Sol. Phys*. 204, 179 (2001)

24. Tabataba-Vakili, F., Grenfell, J. L., Griebmeier, J-M., Rauer, accepted by A& A, arXiV: 1511.04920v1 (2016)

25. Porter, H. S., Jackman, C. H., and Green, A. E. S, *J. Chem. Phys*., 65, 154 (1976)

26. Mlynczak, M. G. and Solomon, S. JGR, 98, D6, 10517 (1993)

27. Garraffo, C., Drake, J. J., Cohen, O. *ApJ*, 833, L4 (2016)

28. Airapetian, V. S., Glocer, A., Khazanov, G. V., Loyd, R. O. P., France, K., Sojka , J., Danchi, W. C. , Liemohn, M. W. *ApJ Let*, 836, L3 (2017)

29. Lei, J., Burns, A. G., Thayer, J. P., Wang, W., Mlynczak, M. G., Hunt, L. A., Dou, X., Sutton, E. JGR, 117, A3, CiteIDA03314 (2012)

30. Arnold, L. et al. A&A, 564, A58 (2014)

31. Porto De Mello, G., Fernandez del Peloso, E., Ghezzi, L. *Astrobiology*, 6, 2 (2006)

32. Cowan, N. B. et al., PASP, 127, 311 (2015).

33. Greene, T. P. et al., ApJ, 817, 17 (2016).

34. Danchi, W.C. & Barry, R. Proc. SPIE, 7734 (2010).

35. Airapetian, V. S., Danchi, W. C., Chen, P. C., Rabin, D. M., Carpenter, K. G., Mlynczak, M. G. in Planetary Science Vision 2050 (2017).

Supplemental Material

1. 2-D GSFC Atmospheric Model.

We employed the Goddard Space Flight Center (GSFC) two-dimensional (2-D) atmospheric model to study the impact of solar protons on the Earth atmospheric chemistry [1,2]. The vertical range of the model is equally spaced in log pressure and extends from the ground to approximately 92 km (0.0024 hPa) with a 1 km grid spacing and 4 degree latitude grid spacing. The transport is computed off-line and is derived using the daily average global winds and temperatures from the NASA Modern Era Retrospective-analysis for Research and Applications (MERRA) meteorological analysis (see the website: http://gmao.gsfc.nasa.gov/research/merra/) for 1979–2012. Thirty-day running averages of the residual circulation, eddy diffusion, zonal mean wind, and zonal mean temperature are computed using the methodology described in [3] and are used as input into the GSFC 2-D model. For this paper, we used the climatological average over the 1979-2012 period for the transport fields. The averaged transport fields change daily, but repeat yearly. .

The ground boundary conditions in the GSFC 2-D model for the source gases are taken from WMO (2011) for year 2000. The model uses a chemical solver described in [3-5]. The photochemical gas and heterogeneous reaction rates and photolysis cross sections have been updated to the Jet Propulsion Laboratory recommendations from year 2010 for these computations [6]. We use the solar proton flux (energies 1 to 300 MeV) for the July 14-16, 2000 SEP event provided by the National Oceanic and Atmospheric Administration (NOAA) Space Weather Prediction Center (SWPC) for the NOAA Geostationary Operational Environmental Satellites (GOES) (see http://www.swpc.noaa.gov/ftpmenu/lists/ particle.html). The GOES 13

data are considered to be the most reliable of the current GOES datasets for the proton fluxes depositing energy into polar latitudes and were used as the source of protons in several energy intervals for the July 2000 SEP event (see also at http://www-istp.gsfc.nasa.gov/istp/events/2000july14/20000716_proton.gif). Peak ionization rates above 10000 cm^{-3} s^{-1} and the energy deposition rate of 5 x 10^{-7} $ergs/cm^3/s$ were reached on July 15, 2000.

The proton flux data were used to compute the ion pair production profiles employing the energy deposition methodology discussed in [7], where the creation of one ion pair was assumed to require 35 eV. The SPE-produced hourly average ionization rates and the energy deposition rates in the polar cap regions (> 60 geomagnetic latitude) are given in Figure 1 and 2, respectively, for July 14-16 of 2000 SEP event. The GOES proton flux during the July 14-16 of 2000 event as well as the impact on the atmosphere is discussed in [8]. We use the daily average ionization rates for July 15, 2000 (the maximum energy deposition day of this SEP event) in the computations shown in the paper.

This model referred to as Model A serves as the reference model for calculation of atmospheric chemistry for Model B with 10 x enhanced XUV flux and Models C, D, and E for 1x, 10x, and 20x of the particles fluxes, respectively.

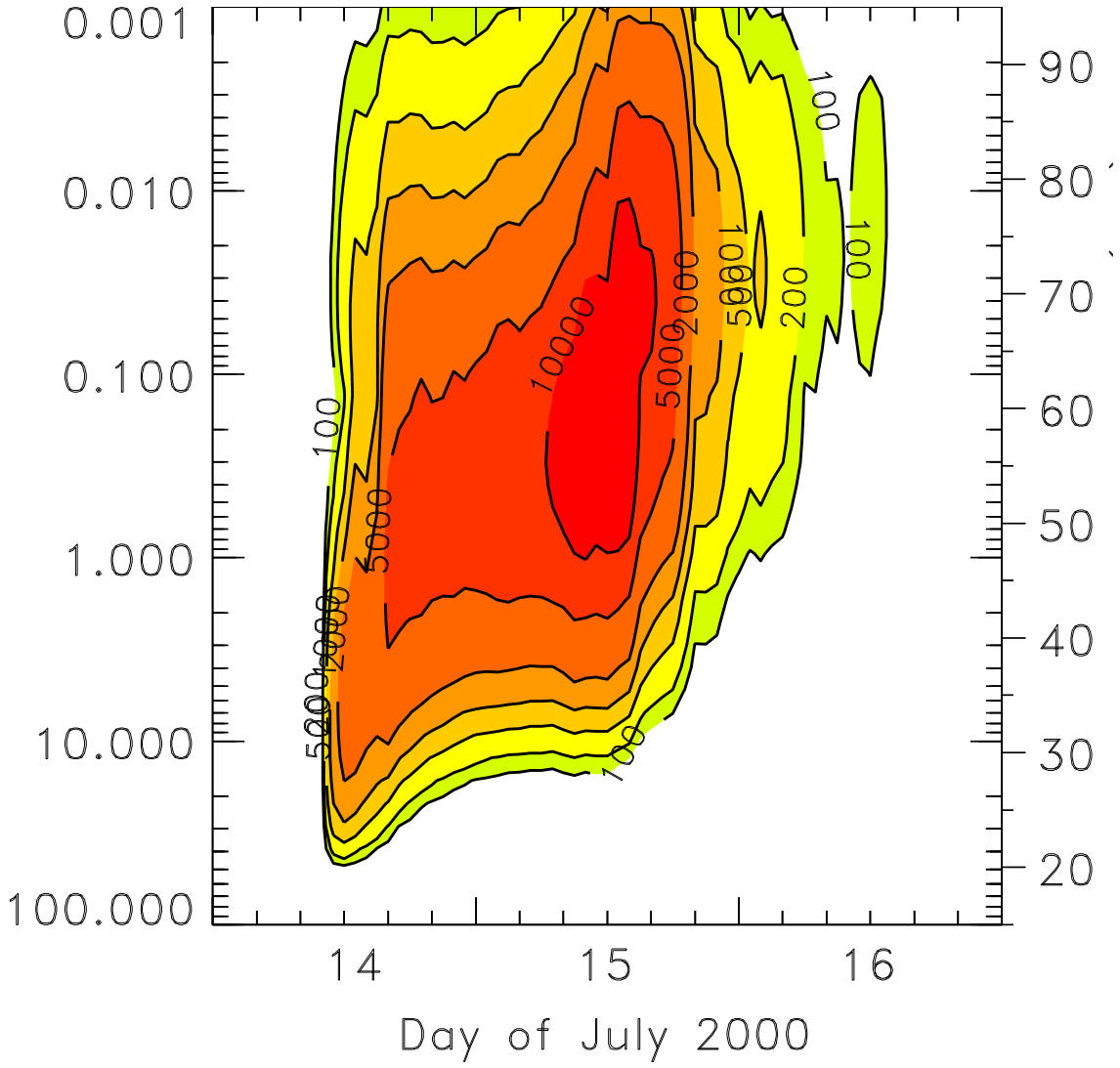

Figure 1. *Ionization rates (in units of # cm^{-3} s^{-1}) for July 2000 SPE event.*

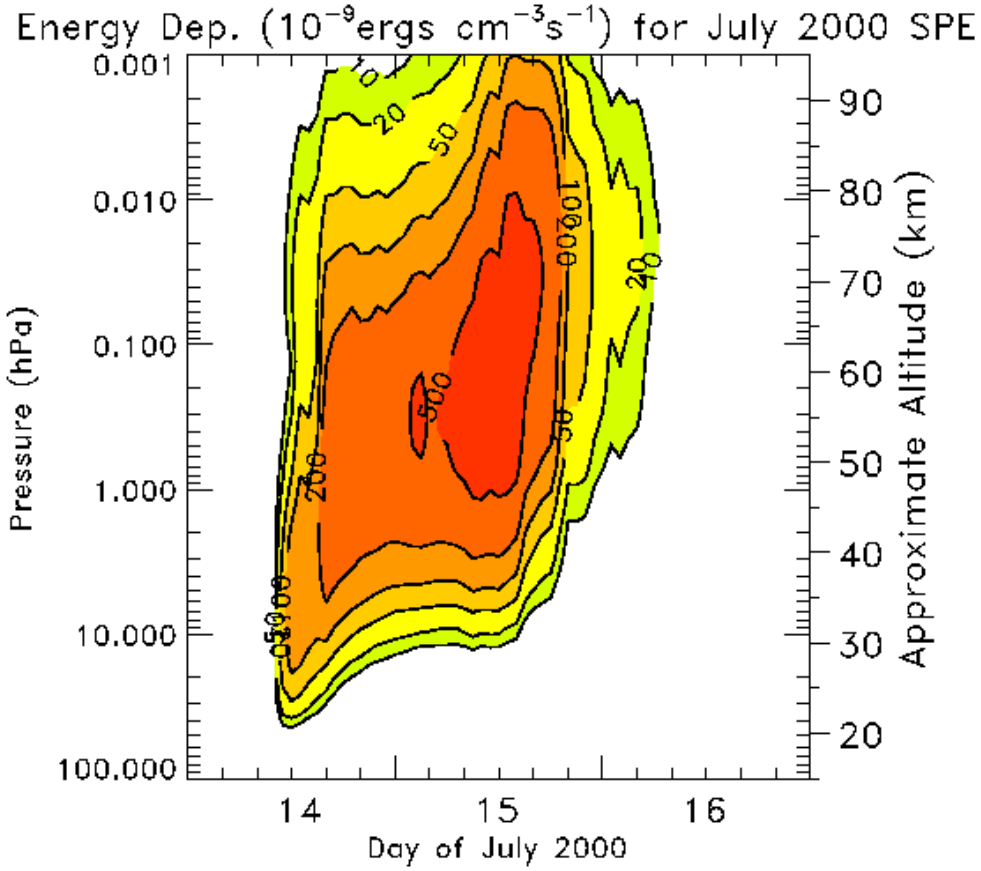

Figure 2. *Energy deposition (in units of 10^{-9} ergs cm^{-3} s^{-1}) for July 2000 SPE.*

2. Production and Destruction of NO and OH

Production and destruction of NO and OH species are driven by the following reactions

$$N_2 + e^- \rightarrow 2N(^4S) + e^- \qquad (R1)$$

$$N_2 + h\nu \rightarrow N(^4S) + N(^2D) \qquad (R2)$$

Other possibilities from this interaction are

$$N_2 + e^- \rightarrow N(^4S) + N(^2D) + e^- \qquad (R3)$$

as well as other products, see [9,10]. The dominant sources of NO production are

$$N(^4S) + O_2 \rightarrow NO + O(^3P) \qquad (R4)$$

$$N(^2D) + O_2 \rightarrow NO + O(^3P) \qquad (R5),$$

and destruction through

$$N(^4S) + NO \rightarrow N_2 + O(^3P). \qquad (R6)$$

(R4) and (R5) are the major sources of production of NO that becomes vibrationally excited by impacts with atomic oxygen in the ionosphere-thermosphere (IT), and thus are temperature dependent. The hydroxyl production is controlled by photolysis of water and collisional dissociation

$$H_2O + Ion^+ \rightarrow H + OH + Ion^+ \qquad (R7)$$

$$H + O_3 \rightarrow OH + O_2 \qquad (R8).$$

2. **Destruction of Thermospheric Ozone.**

   Ozone production comes from the following reactions

$$O_2 + hv\ (<242\ nm) \rightarrow O + O \qquad (R9)$$

   followed by

$$O + O_2 + M \rightarrow O_3 + M \qquad (R10)$$

   Ozone desctruction is mediated via the following reactions

$$O_3 + hv\ (<255\ nm) \rightarrow O_2 + O \qquad (R11)$$

followed by

$$O + O_3 \rightarrow O_2 + O_2 \qquad (R11)$$

Catalytic destruction of ozone is driven by the following reactions

$$O_3 + X \rightarrow XO + O_2 \quad (X=O, NO, OH, Br \text{ or } Cl) \qquad (R12)$$

$$O + XO \rightarrow X + O_2 \qquad (R13)$$

$$Net: O + O_3 \rightarrow O_2 + O_2 \qquad (R14)$$

X is not destroyed but continuously participate in the cylcle.

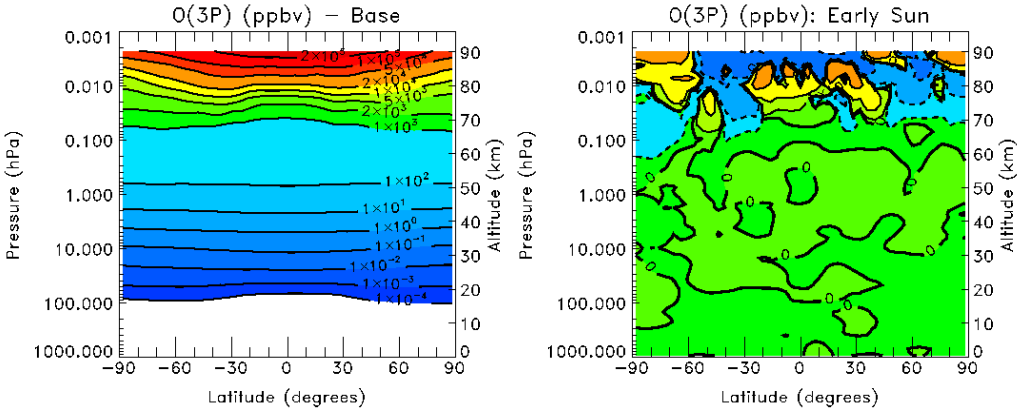

Figure 3 shows the 2D map of atomic oxygen O(^{3}P) produced by photolysis driven by XUV flux from a young active star (right panel; Model B) with respect to the base model (left panel; Model A).

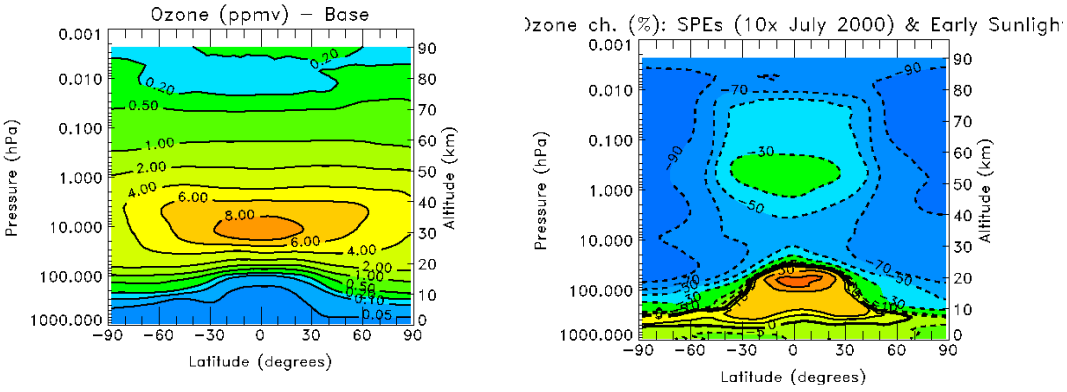

Figure 4 presents the 2D map of atmospheric ozone destruction driven by XUV flux from an active star and a10xJuly 2000 SEP event (right panel, Model D) with respect to the base model (left panel; Model A).

References.

1. Douglass, A. R., Jackman, C. H., and Stolarski, R. S. *JGR*, 94, 9862, 1989.
2. Jackman, C. H., Randall, C. E., Harvey, V. L., Wang, S., Fleming, E. L., M. López-Puertas, M., Funke, B. and P. F. Bernath, P F. *Atmos*. *Chem*. *Phys*. 14, 1025 (2014)
3. Fleming, E. L., Jackman, C. H., Weisenstein, D. K., and Ko, M. K. W. *JGR*, 112, D10310, doi:10.1029/2006JD007953, 2007.
4. Jackman, C. H., DeLand, M. T., Labow, G. J., Fleming, E. L., Weisenstein, D. K., Ko, M. K. W., Sinnhuber, M., and Russell, J. M. *JGR*, 100, A09S27,doi:10.1029/2004JA010888, 2005.

5. Fleming, E. L., Jackman, C. H., Stolarski, R. S., Douglass, A. R. Atm. Chem. Phys., 11, 8515 (2011)
6. Sander, S. P., Friedl, R. R., Barker, J. R., Golden, D. M., Kurylo, M. J., Wine, P. H., Abbatt, J. P. D., Burkholder, J. B., Kolb, C. E., Moortgat, G. K., Huie, R. K., and Orkin, V. L. Chemical kinetics and photochemical data for use in atmospheric studies, Evaluation Number 17, JPL Publication 10-6, 2010.
7. Jackman, C. H., Frederick, J. E., and Stolarski, R. S, *JGR*, 85, 7495, 1980.
8. Jackman, C. H., McPeters, R. D., Labow, G. J., Fleming, E. L., Praderas, C. J., Russell, J. M., GRL, 28, 2883, 2001.
9. Rodgers, E. M., Bailey, S. M., Warren, H. P., Woods, T. N., Eparvier, F. G. Adv. Space Res., 45, 28 (2010)
10. Vitt, F. M.; Armstrong, T. P.; Cravens, T. E.; Dreschhoff, A. M.; Jackman, C. H.; Laied, C. M. *J. Atmos. Sol.-Terr. Phys.*, 62, No. 8, 669 (2000)